Developing a global indicator for Aichi Target 1 by merging online data sources to measure biodiversity awareness and engagement

Cooper, Matthew W.

2019-02

Cooper , M W , Di Minin , E , Hausmann , A , Qin , S , Schwartz , A J & Correia , R A 2019 , ' Developing a global indicator for Aichi Target 1 by merging online data sources to measure biodiversity awareness and engagement ' , Biological Conservation , vol. 230 , pp. 29-36 . https://doi.org/10.1016/j.bi

http://hdl.handle.net/10138/322843
https://doi.org/10.1016/j.biocon.2018.12.004

Effect of the interspecies interaction on the density profiles of miscible two-species Bose–Einstein condensates

P. Kuopanportti,[1] Y. M. Liu,[2] Y. Z. He,[3] and C. G. Bao[3]

[1]*Department of Physics, University of Helsinki, P.O. Box 43, FI-00014 Helsinki, Finland*
[2]*Department of Physics, Shaoguan University, Shaoguan, 512005, China*
[3]*School of Physics, Sun Yat-Sen University, Guangzhou, 510275, China*

(Dated: November 9, 2018)

We study harmonically trapped two-species Bose–Einstein condensates within the Gross–Pitaevskii formalism. By invoking the Thomas–Fermi approximation, we derive an analytical solution for the miscible ground state in a particular region of the system's parameter space. This solution furnishes a simple formula that relates the interspecies interaction strength to the second spatial moments of the density distribution of the minority condensate species. Accompanying numerical simulations confirm the accuracy of the solution and the interaction-strength formula for sufficiently large numbers of condensed particles. The introduced formula may provide an additional scheme for determining interspecies scattering lengths that complements existing methods, such as those based on collective-excitation spectroscopy of the two-species condensates or on collisional measurements on thermal samples.

PACS numbers: 03.75.Mn, 67.85.Fg, 03.75.Hh
Keywords: Bose–Einstein condensation, Multicomponent condensate, Thomas–Fermi approximation

I. INTRODUCTION

Binary mixtures of Bose–Einstein condensates (BECs) have been extensively studied in recent years, both experimentally and theoretically. In experiments to date, these so-called two-species BECs have been produced by using either two different elements [1–10], two distinct isotopes of the same element [11–13], or a single isotope in two different internal states [14–19]. Theoretical studies, in turn, have addressed diverse phenomena such as segregation [20–24] and the associated symmetry breaking [25–29], wetting phase transitions [30], and exotic vortex structures [31–40], to name but a few.

A key ingredient that gives rise to these phenomena and sets the two-species system apart from the single-species BEC is, quite obviously, the interspecies interaction, which is taken here to be of the zero-range density–density type. It can have a drastic effect on the ground-state density distributions, leading, for example, to segregation of the two condensates when it is strongly repulsive [6, 10, 11]. In this paper, we demonstrate how the ground-state shapes of the coupled condensates encode crucial information about the interspecies interaction, even when no phase separation occurs, and how the information can be conveniently extracted. Specifically, based on the analytical Thomas–Fermi (TF) formalism, we derive a ground-state solution of the system in closed form and, as a corollary, a simple formula [Eq. (17)] that can be used to determine the relative strength of the interspecies interaction from the knowledge of the density distribution of just one of the two miscible condensate species.

The rest of the article is organized as follows. We present the Gross–Pitaevskii (GP) equations of the two-species BEC in Sec. II and solve them analytically within the TF approximation (TFA) in Sec. III. The analytical solution is then utilized in Sec. IV to investigate the behavior of the density profiles as a function of the interspecies interaction strength. Section V presents the derivation of the aforementioned interaction-strength formula. In Sec. VI, we use direct numerical solutions of the GP equations to test the accuracy of the interaction-strength formula outside the TFA. Section VII summarizes our main findings and discusses limitations and possible future extensions of the work.

II. GROSS–PITAEVSKII MODEL

As the starting point of our theoretical treatment, let N_A bosonic atoms of species A and mass m_A and N_B bosonic atoms of species B and mass m_B be confined and Bose–Einstein condensed in three-dimensional, concentric harmonic traps. Atoms within each species are assumed to interact weakly through repulsive contact interaction of strength $c_S = 4\pi\hbar^2 a_{SS}/m_S > 0$, where $S \in \{A, B\}$ and a_{SS} is the s-wave scattering length between atoms of species S. The interspecies contact interaction strength $c_{AB} = 2\pi\hbar^2 a_{AB}(m_A^{-1} + m_B^{-1})$, where a_{AB} is the positive or negative interspecies s-wave scattering length, is taken to be weak enough for the two species to remain miscible [41]. The concentric harmonic traps are written as $V^S_{\text{trap}}(\mathbf{r}) = m_S(\omega^2_{Sx}x^2 + \omega^2_{Sy}y^2 + \omega^2_{Sz}z^2)/2$, where the trap frequencies ω_{Sl}, $l \in \{x, y, z\}$, may all be different [42]. It should be noted, however, that we have assumed the two traps to be co-aligned such that they can both be assigned the same symmetry axes (which we have selected as our Cartesian coordinate axes).

For the sake of convenience and notational symmetry, we introduce a mass m and a frequency ω and hereafter use $\hbar\omega$ and $a_{\text{osc}} \equiv \sqrt{\hbar/(m\omega)}$ as units of energy and length, respectively. Assuming that the atomic clouds of both species are dilute and that the temperature is close enough to zero, the ground state of the two-species BEC can be described accurately by the time-independent coupled GP equations [43–45]

for the condensate wave functions ϕ_S, $S \in \{A, B\}$:

$$\Big[-\frac{m}{2m_S}\nabla^2 + \frac{1}{2}\left(\gamma_{Sx}x^2 + \gamma_{Sy}y^2 + \gamma_{Sz}z^2\right) + \alpha_S|\phi_S(\mathbf{r})|^2 + \beta_S|\phi_{\not S}(\mathbf{r})|^2 - \mu_S\Big]\phi_S(\mathbf{r}) = 0, \tag{1}$$

where $\gamma_{Sl} = m_S\omega_{Sl}^2/(m\omega^2)$ is a dimensionless trap-strength parameter, $\not S$ is defined such that $\not A = B$ and $\not B = A$, the dimensionless coupling constants are

$$\alpha_S = 4\pi N_S \frac{m a_{SS}}{m_S a_{\mathrm{osc}}}, \tag{2}$$

$$\beta_S = 2\pi N_S \frac{m(m_A + m_B)a_{AB}}{m_A m_B a_{\mathrm{osc}}}, \tag{3}$$

and μ_S are the chemical potentials that enter as Lagrange multipliers enforcing the unit normalization $\int_{\mathbb{R}^3}|\phi_S^2(\mathbf{r})|\,\mathrm{d}^3r = 1$. In this notation, the number density of atoms in the BEC of species S is written as $N_S|\phi_S|^2$. Since we will only consider flowless ground states, we can assume ϕ_S to be real valued.

III. THOMAS–FERMI SOLUTION

We now introduce the TFA [45–47], which applies to sufficiently large numbers of condensed atoms and amounts to neglecting the kinetic-energy terms in the GP equations [48]. When both ϕ_A and ϕ_B are nonzero, the resulting TF versions of Eqs. (1) can be written as

$$\alpha_S\phi_S^2 + \beta_S\phi_{\not S}^2 = \mu_S - \frac{1}{2}\left(\gamma_{Sx}x^2 + \gamma_{Sy}y^2 + \gamma_{Sz}z^2\right). \tag{4}$$

If the determinant $D \equiv \alpha_A\alpha_B - \beta_A\beta_B \neq 0$, we obtain

$$\phi_S^2 = X_S - Y_{Sx}x^2 - Y_{Sy}y^2 - Y_{Sz}z^2, \tag{5}$$

where

$$X_S \equiv (\alpha_{\not S}\mu_S - \beta_S\mu_{\not S})/D, \tag{6}$$

$$Y_{Sl} \equiv (\alpha_{\not S}\gamma_{Sl} - \beta_S\gamma_{\not S l})/(2D). \tag{7}$$

We will refer to the formal solution given by Eqs. (5) as Form II. Equations (6) can be solved for the chemical potentials:

$$\mu_S = \alpha_S X_S + \beta_S X_{\not S}. \tag{8}$$

The parameters Y_{Sl} defined in Eqs. (7) are known once the input parameters are given, while X_S remain unknown because they depend on μ_S.

If exactly one of the two wave functions, say ϕ_A, is zero in a certain region of $\mathbb{R}^3$, the formal solution is

$$\phi_A = 0, \tag{9a}$$

$$\phi_B^2 = \frac{1}{\alpha_B}\left[\mu_B - \frac{1}{2}\left(\gamma_{Bx}x^2 + \gamma_{By}y^2 + \gamma_{Bz}z^2\right)\right]. \tag{9b}$$

A solution of this type is referred to as Form I_B, where the subscript B indicates the nonvanishing species. Analogously, Form I_A can be defined. Together with the vacuum $\phi_A = \phi_B = 0$, Forms I_A, I_B, and II exhaust all possible types of local TF solutions of Eqs. (1).

If one of the wave functions in Form II, say $\phi_A(\mathbf{r})$, reaches zero as we vary $\mathbf{r}$, we arrive at a boundary surface of Form II (for instance, ϕ_A will reach zero upon increasing x sufficiently if $Y_{Ax} > 0$). Crossing the boundary will lead to a transformation from Form II to Form I_B. It is emphasized that both wave functions are always continuous at the form boundaries; this is because the equations governing the two neighbouring forms become exactly the same for the boundary points. In this way the formal solutions, each with its own specific domain of definition, will be naturally and continuously linked up to form the complete piecewise-defined TF solution over entire $\mathbb{R}^3$. The complete TF wave functions, however, will not in general be differentiable at the form boundaries. The two unknowns μ_S appearing in the entire solution can be obtained from the two additional equations $\int_{\mathbb{R}^3}\phi_S^2\,\mathrm{d}^3r = 1$ for normalization.

The parameter space of the two-species model is fairly high-dimensional: even after all the redundancies are removed, one must specify the values of at least nine independent parameters in order to fix all the coefficients in Eqs. (1). Partly for this reason, we will not develop the general TF solution any further in what follows. Instead, for our purposes, it is sufficient to consider a specific type of TF solution satisfying the following assumptions: (i) The isosurfaces of ϕ_A^2 are ellipsoids, and ϕ_A^2 has its maximum at the origin. (ii) $\phi_B^2 > 0$ if $\phi_A^2 > 0$. (iii) The boundary surfaces of the two condensates do not have any points in common. A TF solution satisfying assumptions (i)–(iii) will approximate the ground state of the system in a particular region of the whole parameter space. Note that these assumptions are different for the two species and hence should be used as the criteria for assigning the two labels A and B.

Due to assumptions (i) and (ii), the solution has Form II at the origin, and it follows from Eqs. (5) that $X_A = \phi_A^2(\mathbf{r} = \mathbf{0}) > 0$ and $X_B = \phi_B^2(\mathbf{r} = \mathbf{0}) > 0$. Assumption (i) also implies that all the three $Y_{Al} > 0$. Let us refer to the region in which ϕ_A remains nonzero as the inner region, $\Omega_{\mathrm{in}} \equiv \left\{(x, y, z) \in \mathbb{R}^3 \mid \sum_l Y_{Al}l^2 < X_A\right\}$. We know from assumption (ii) that the solution has Form II in Ω_{in} and from assumption (iii) that ϕ_B^2 remains positive on the boundary ellipsoid $\partial\Omega_{\mathrm{in}}$. As we cross $\partial\Omega_{\mathrm{in}}$ to the outside, the solution acquires Form I_B [Eqs. (9)]. Since all the three γ_{Bl} are positive by definition, the isosurfaces of ϕ_B^2 in Eq. (9b) are also ellipsoids, and ϕ_B^2 will reach zero on the ellipsoid $\left\{(x, y, z) \in \mathbb{R}^3 \mid \sum_l \gamma_{Bl}l^2 = 2\mu_B\right\} \equiv \mathcal{S}$. Because both wave functions vanish outside $\mathcal{S}$, it is the boundary surface of the whole two-species BEC. The region between $\partial\Omega_{\mathrm{in}}$ and $\mathcal{S}$ is referred to as the outer region and denoted by Ω_{out}.

The normalization $1 = \int_{\mathbb{R}^3}\phi_A^2\,\mathrm{d}^3r = \int_{\Omega_{\mathrm{in}}}\phi_A^2\,\mathrm{d}^3r$ yields

$$X_A = \left(\frac{15\sqrt{Y_{Ax}Y_{Ay}Y_{Az}}}{8\pi}\right)^{2/5}. \tag{10}$$

From the normalization $1 = \int_{\mathbb{R}^3}\phi_B^2\,\mathrm{d}^3r = \int_{\bar{\Omega}_{\mathrm{in}}\cup\bar{\Omega}_{\mathrm{out}}}\phi_B^2\,\mathrm{d}^3r$ and

Eqs. (8) and (10), we obtain

$$\frac{\mu_B^{5/2}}{15} = \frac{\prod_l \gamma_{Bl}^{1/2}}{16\sqrt{2}\pi}\left(\alpha_B + \frac{5}{2}\beta_B + \sum_l \frac{2\alpha_B Y_{Bl} - \gamma_{Bl}}{4Y_{Al}}\right). \quad (11)$$

We can further use Eqs. (6) and (8) to write down closed-form expressions for the remaining unknowns $X_B = (\mu_B - \beta_B X_A)/\alpha_B$ and $\mu_A = (DX_A + \beta_A \mu_B)/\alpha_B$. Thus, all the quantities involved in ϕ_A and ϕ_B have now been determined in terms of the model input parameters, and thereby the desired TF solution has been obtained.

In order for the solution to be self-consistent, it must satisfy the assumptions made in its design. Since we must necessarily have

$$Y_{Ax} > 0, \quad Y_{Ay} > 0, \quad Y_{Az} > 0, \quad (12)$$

the requirement $X_A > 0$ is immediately satisfied by Eq. (10). By utilizing standard techniques of analytical minimization, we can cast the constraint $\phi_B^2(\mathbf{r}) > 0 \ \forall \mathbf{r} \in \bar{\Omega}_{\rm in}$, where ϕ_B^2 is given by Eq. (5), as the inequality

$$\frac{X_B}{X_A} > \max\left\{0, \max_l \frac{Y_{Bl}}{Y_{Al}}\right\}. \quad (13)$$

Furthermore, assumption (iii) implies that ϕ_B^2 as given by Eq. (9b) must be positive on $\partial\Omega_{\rm in}$, which in turn requires that

$$\mu_B > \frac{X_A}{2} \max_l \frac{\gamma_{Bl}}{Y_{Al}}. \quad (14)$$

As long as the ten input parameters γ_{Sl}, α_S, and β_S are chosen such that the inequalities (12)–(14) are satisfied, the TF solution derived above is self-consistent.

It is worth noting that when the interspecies coupling c_{AB} vanishes, the above solution reduces to the well-known single-species case, $\phi_S^2(\mathbf{r}) = \max\{0, (\mu_S - \frac{1}{2}\sum_l \gamma_{Sl} l^2)/\alpha_A\}$, where $\mu_S = \frac{1}{2}\left[15\alpha_S \prod_l \gamma_{Sl}/(4\pi)\right]^{2/5}$ [49]. Similarly, by assuming that both harmonic traps are spherically symmetric ($\omega_{Sx} = \omega_{Sy} = \omega_{Sz}$), we recover the radial wave functions presented in Refs. [50, 51].

IV. EFFECT OF THE INTERSPECIES INTERACTIONS ON THE DENSITY PROFILES

As an example of how our analytical TF solution can be used to infer properties of the harmonically trapped miscible two-species BEC, let us consider the effect of the interspecies interactions on the ground-state density profiles. To this end, Fig. 1 shows the TF wave functions for five different interspecies interaction strengths c_{AB}. While c_{AB} is varied here primarily for the sake of illustration, in experiments its value could be manipulated using Feshbach resonances [52], which have been demonstrated for, e.g., ^{87}Rb–^{87}Rb [53–55], ^{41}K–^{41}K [56, 57], and ^{87}Rb–^{41}K [3] interactions. The accuracy of the TFA will be assessed in Sec. VI.

Since we have chosen $\omega_{Az} > \omega_{Ax} = \omega_{Ay}$ and $\omega_{Bz} > \omega_{Bx} = \omega_{By}$, the atomic clouds of both species are oblate. Moreover,

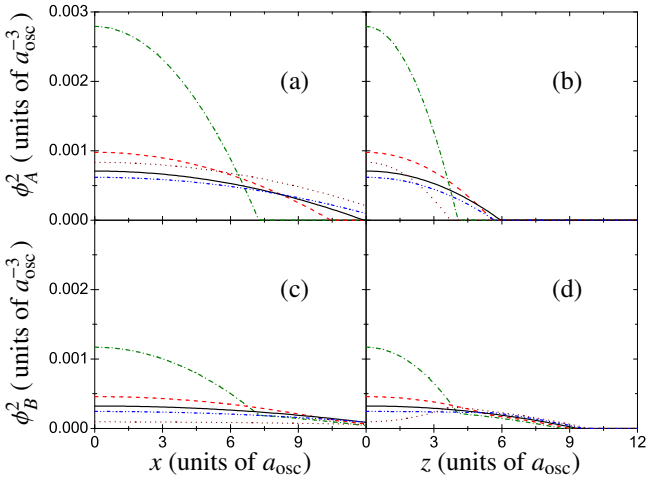

Figure 1. Thomas–Fermi solutions for ϕ_A^2 along (a) the x and (b) the z axes and for ϕ_B^2 along (c) the x and (d) the z axes, for five different values of the interspecies interaction strength c_{AB}: $-1.032 \times c_A$ (dash-dotted curves), $-1.032 \times c_A/2$ (dashed), 0 (solid), $1.032 \times c_A/2$ (dash-dot-dotted), and $1.032 \times c_A$ (dotted). The system is rotationally symmetric about the z axis ($\omega_{Ax} = \omega_{Ay}$ and $\omega_{Bx} = \omega_{By}$), and the unit of length is $a_{\rm osc} = \sqrt{\hbar/(m_A\omega_{Ax})}$. For all five solutions, we have used the parameter values $m_B/m_A = 0.471$ and $c_B/c_A = 1.29$, which correspond to species A being ^{87}Rb and species B being ^{41}K, along with $N_B/N_A = 2.5$, $\omega_{Bx}/\omega_{Ax} = 1.5$, $\omega_{Az}/\omega_{Ax} = 2$, $\omega_{Bz}/\omega_{Bx} = 1.5$, and $\alpha_A = 10^5$. The dotted curves ($c_{AB}/c_A = 1.032$) correspond to the natural s-wave scattering length between ^{87}Rb and ^{41}K without Feshbach-resonance manipulation.

because $\alpha_B > \alpha_A$, the atoms of species B are subjected to stronger intraspecies repulsion than the atoms of species A; consequently, the species-B cloud extends further away from the origin and contains the entire species-A cloud. This inherent size difference, which is implied by assumptions (ii) and (iii) made about our TF solution, is evident for the uncoupled system with $c_{AB} = 0$ (solid curves in Fig. 1).

Since both condensate species are present in the inner region $\Omega_{\rm in}$, atoms of one species are affected by atoms of the other species if the interspecies interaction is turned on. When this coupling is attractive ($c_{AB} < 0$), both clouds tend to shrink in order to increase their mutual overlap and thereby enhance the attractive interspecies interaction energy $E_{AB} = c_{AB}N_AN_B\int_{\mathbb{R}^3}\phi_A^2\phi_B^2\,{\rm d}^3r < 0$. The size reduction with growing interspecies attraction can be discerned from Fig. 1 by observing the progression from solid to dashed to dash-dotted curves. Nevertheless, some of the species-B atoms remain outside the species-A cloud in the outer region $\Omega_{\rm out}$, and the distribution of species B develops into a central bump surrounded by a long tail [dash-dotted curves in Figs. 1(c) and 1(d)].

In contrast, when the interspecies coupling is repulsive ($c_{AB} > 0$), the two species tend to avoid each other so as to minimize the positive interspecies interaction energy E_{AB}. As evidenced by the progression from solid to dash-dot-dotted to dotted curves in Figs. 1(a) and 1(b), the cloud of species A becomes more oblate with increasing c_{AB}, with ϕ_A^2 concentrated at small $|z|$. At the same time, the species-B density becomes

depleted at small $|z|$ [dotted curve in Fig. 1(d)], which causes the maximum point of ϕ_B^2 to shift from the origin to the two points $(x, y, z) = (0, 0, \pm\sqrt{X_A/Y_{Az}}) \in \partial\Omega_{\rm in}$.

The above discussion illustrates that changes in the interspecies interaction strength c_{AB} can cause significant changes in the shapes of the two atomic clouds, even while remaining in the miscible regime. As shown in the next section, information on c_{AB} can be directly extracted from the second spatial moments of the probability density distributions—in fact, it is enough to know them for just one of the two species.

V. INTERACTION-STRENGTH FORMULA

It turns out that the relative strength of the interspecies interaction can be determined by observing only the inner cloud, i.e., the density distribution of species A. The mean square value of the atomic coordinate $l \in \{x, y, z\}$ in the species-A cloud is

$$\langle l^2\rangle_A \equiv \int_{\mathbb{R}^3} |\phi_A^2|\, l^2 \mathrm{d}^3 r = \left(\frac{15}{8\pi}\right)^{2/5} \frac{Y_{Ax}^{1/5} Y_{Ay}^{1/5} Y_{Az}^{1/5}}{7\, Y_{Al}}. \tag{15}$$

Furthermore, we define a 3-by-3 matrix δ^A with elements

$$\delta^A_{ll'} \equiv \langle l^2\rangle_A / \langle l'^2\rangle_A = Y_{Al'}/Y_{Al}, \tag{16}$$

where $l, l' \in \{x, y, z\}$. For the case $\gamma_{Al'}/\gamma_{Al} \neq \gamma_{Bl'}/\gamma_{Bl}$, we can, by using Eqs. (7), rewrite Eq. (16) as

$$\frac{c_{AB}}{c_B} = \frac{m_A}{m_B} \frac{\omega_{Al'}^2 - \omega_{Al}^2 \delta^A_{ll'}}{\omega_{Bl'}^2 - \omega_{Bl}^2 \delta^A_{ll'}} \qquad \left(\frac{\omega_{Al'}}{\omega_{Al}} \neq \frac{\omega_{Bl'}}{\omega_{Bl}}\right). \tag{17}$$

If the atomic masses and trap frequencies are known, Eq. (17) can be used to determine the relative strength of the interspecies interaction from the mean-square values of any two coordinates in the density distribution of species A only. As such, Eq. (17) may provide a means to determine c_{AB} that could complement existing methods based on collective-excitation spectroscopy of the binary BEC [58] or on collisional measurements on thermal samples [1, 59].

It is also interesting to note that Eq. (17) implies some nontrivial relations between the elements of the matrix δ^A. For instance, if a two-species system describable by our TF solution satisfies the condition $\omega_{Al'}/\omega_{Al} \neq \omega_{Bl'}/\omega_{Bl}$ for all three coordinate pairs $(l, l') \in \{(x, y), (x, z), (y, z)\}$, we then have

$$\begin{aligned} &\left(\omega_{Ay}^2 - \omega_{Ax}^2\delta^A_{xy}\right)\left(\omega_{Bz}^2 - \omega_{Bx}^2\delta^A_{xz}\right)\left(\omega_{Bz}^2 - \omega_{By}^2\delta^A_{yz}\right) \\ &= \left(\omega_{By}^2 - \omega_{Bx}^2\delta^A_{xy}\right)\left(\omega_{Az}^2 - \omega_{Ax}^2\delta^A_{xz}\right)\left(\omega_{Bz}^2 - \omega_{By}^2\delta^A_{yz}\right) \\ &= \left(\omega_{By}^2 - \omega_{Bx}^2\delta^A_{xy}\right)\left(\omega_{Bz}^2 - \omega_{Bx}^2\delta^A_{xz}\right)\left(\omega_{Az}^2 - \omega_{Ay}^2\delta^A_{yz}\right). \end{aligned} \tag{18}$$

In analogy with Eq. (15), our TF solution makes it possible to derive an approximate analytical expression for any observable that can be written as a functional of the BEC ground-state wave functions ϕ_A and ϕ_B. The resulting expressions for the observables as functions of the model parameters could then be used in numerical optimization to fit against experimental data and in this way infer the values of unknown model parameters, without having to resort to computationally demanding three-dimensional GP simulations that are typically needed for triaxial harmonic traps. The usefulness of this approach of course hinges on the accuracy of the TFA, which we will assess in the next section.

VI. COMPARISON WITH NUMERICAL RESULTS

The formulae presented in Sec. III are generalizations to triaxial configurations of previously obtained expressions for spherically symmetric harmonic traps [24, 26, 50, 51]. They, as well as Eqs. (15)–(17), are all based on the TFA and will therefore inherit its errors. However, the TFA is known to become more accurate with increasing number of atoms. It is therefore natural to ask how large condensates one would need in order for the approximation error to be negligible. To answer this question, we perform numerical calculations beyond the TFA to obtain the essentially exact ground-state solutions of the GP equations (1). We further define $(c_{AB}/c_B)_{\rm est}$ as the *estimate* obtained from Eq. (17) by replacing the TF value of $\delta^A_{ll'}$ with that of the numerical solution. When the relative error of this estimate is negligible, Eq. (17) is applicable for the determination of c_{AB}/c_B.

In our numerical calculations, we discretize Eqs. (1) by applying the standard three-point finite-difference stencil and solve the resulting equations iteratively with the successive overrelaxation algorithm. We use coordinate grids with step lengths $\leq 0.05 \times \sqrt{\hbar/(m_A\omega_{Ax})}$ in each direction. To enable simple visualization, we set $\omega_{Ax} = \omega_{Ay}$ and $\omega_{Bx} = \omega_{By}$ and limit the simulations to cases where both ϕ_A^2 and ϕ_B^2 are rotationally symmetric about the z axis. We stress, however, that our analytical treatment also applies to two-species BECs with no cylindrical symmetry.

Table I collects our numerical results for a two-species BEC where the two condensates are coupled through a repulsive interspecies interaction of relative strength $c_{AB}/c_B = 0.8$ and confined in cylindrically symmetric oblate harmonic traps (i.e., $\omega_{Sz} > \omega_{Sx} = \omega_{Sy}$). The table entries correspond to different values of $\alpha_A \propto N_A$, while the other system parameters are kept constant as described in the table caption. The analytical TF and the numerical GP solutions for the entry with $\alpha_A = 10^5$ are presented in Fig. 2; the same TF wave functions are also shown by the dotted curves in Fig. 1. For the smallest four values of α_A in Table I, the root-mean-square (RMS) values $\sqrt{\langle x^2\rangle_A}$ and $\sqrt{\langle z^2\rangle_A}$ show a noticeable discrepancy between the numerical GP solution and the TFA; consequently, for these states $(c_{AB}/c_B)_{\rm est}$ differs significantly from the true value 0.8. However, when α_A increases above 10^4, the accuracy of the TFA improves, the values of $\sqrt{\langle x^2\rangle_A}$ and $\sqrt{\langle z^2\rangle_A}$ computed for the numerical solution approach their TF limits, and $(c_{AB}/c_B)_{\rm est}$ becomes very close to 0.8. For $\alpha_A = 10^6$, for instance, $(c_{AB}/c_B)_{\rm est}$ has a relative error of -0.239% only.

Table II lists the corresponding results for a case where both harmonic traps are prolate ($\omega_{Sz} < \omega_{Sx}$) and there is a fairly strong interspecies repulsion of $c_{AB}/c_B = 1.06$ [60]. The analytical and numerical solutions are presented in Fig. 3 for $\alpha_A = 10^4$. Despite the prolate trap with $\omega_{Az}/\omega_{Ax} = 0.8$, the

Table I. RMS values of the coordinates x and z for ground-state density distribution of a harmonically trapped, three-dimensional two-species BEC with $N_B/N_A = 2.5$, $c_{AB}/c_A = 1.032$, $\omega_{Bx}/\omega_{Ax} = 1.5$, $\omega_{Az}/\omega_{Ax} = 2$, $\omega_{Bz}/\omega_{Bx} = 1.5$, and $\omega_{Ay}/\omega_{Ax} = \omega_{By}/\omega_{Bx} = 1$. The RMS values are given for both the numerically obtained GP solution and the Thomas–Fermi approximation (TFA) derived in the text. The second-to-last column shows the estimate $(c_{AB}/c_B)_{\rm est}$ for the relative interspecies interaction strength, which is obtained by evaluating the right-hand side of Eq. (17) for the numerically obtained ϕ_A. The last column gives the relative error of $(c_{AB}/c_B)_{\rm est}$. For the TFA, Eq. (17) is exact and yields the true value $c_{AB}/c_B = 0.8$. We have used the values $m_B/m_A = 0.471$ and $c_B/c_A = 1.29$, which correspond to species A being ^{87}Rb and species B being ^{41}K. The first column shows the value of the intraspecies interaction strength for species A, $\alpha_A = N_A c_A/(\hbar\omega a_{\rm osc}^3) = 4\pi N_A a_{AA}/a_{\rm osc}$, where $a_{\rm osc} = \sqrt{\hbar/(m\omega)}$, $m = m_A$, and $\omega = \omega_{Ax}$. All lengths are given in units of $a_{\rm osc}$. (If we use $\omega = 2\pi \times 100$ Hz and $a_{AA} = 99\, a_{\rm B}$, we obtain $a_{\rm osc} \approx 1.1\ \mu$m and $\alpha_A \approx 0.061 \times N_A$.) All the listed states satisfy inequalities (12)–(14), rendering our TF solution self-consistent.

	$\langle x^2\rangle_A^{1/2}$		$\langle x^2\rangle_B^{1/2}$		$\langle z^2\rangle_A^{1/2}$		$\langle z^2\rangle_B^{1/2}$		$(c_{AB}/c_B)_{\rm est}$	
α_A	Numer.	TFA	Numer.	TFA	Numer.	TFA	Numer.	TFA	Value	Error (%)
10^0	0.7100	0.5230	0.7618	0.5724	0.5020	0.1410	0.5998	0.4221	7.5553	844.409
10^1	0.9312	0.8289	1.0170	0.9072	0.5605	0.2235	0.7880	0.6689	−2.2950	−386.881
10^2	1.4346	1.3136	1.4392	1.4378	0.6500	0.3543	1.0822	1.0602	0.3135	−60.807
10^3	2.1923	2.0820	2.2500	2.2788	0.7574	0.5615	1.6809	1.6803	0.6742	−15.725
10^4	3.3380	3.2997	3.5994	3.6117	0.9883	0.8899	2.6607	2.6632	0.7633	−4.589
10^5	5.2336	5.2297	5.7226	5.7241	1.4478	1.4104	4.2194	4.2208	0.7909	−1.131
10^6	8.2869	8.2885	9.0725	9.0720	2.2474	2.2354	6.6891	6.6896	0.7981	−0.239
10^7	13.1356	13.1364	14.3785	14.3782	3.5464	3.5429	10.6021	10.6022	0.7996	−0.046

Table II. RMS values of the coordinates x and z in the ground-state density distribution and the corresponding estimates $(c_{AB}/c_B)_{\rm est}$ for a harmonically trapped, three-dimensional two-species BEC with $N_B/N_A = 20$, $c_{AB}/c_A = 0.8217$, $\omega_{Bx}/\omega_{Ax} = 0.65$, $\omega_{Az}/\omega_{Ax} = 0.8$, $\omega_{Bz}/\omega_{Bx} = 0.6$, and $\omega_{Ay}/\omega_{Ax} = \omega_{By}/\omega_{Bx} = 1$. We have used the values $m_A/m_B = 0.471$ and $c_A/c_B = 1.29$, which correspond to species A being ^{41}K and species B being ^{87}Rb. The first column shows the value of the intraspecies interaction strength for species A, $\alpha_A = N_A c_A/(\hbar\omega a_{\rm osc}^3) = 4\pi N_A a_{AA}/a_{\rm osc}$, where $a_{\rm osc} = \sqrt{\hbar/(m\omega)}$, $m = m_A$, and $\omega = \omega_{Ax}$. (If we use $\omega = 2\pi \times 100$ Hz and $a_{AA} = 60\, a_{\rm B}$, we obtain $a_{\rm osc} \approx 1.57\ \mu$m and $\alpha_A \approx 0.0254 \times N_A$.) All lengths are given in units of $a_{\rm osc}$, and the true value for c_{AB}/c_B is exactly 1.06.

	$\langle x^2\rangle_A^{1/2}$		$\langle x^2\rangle_B^{1/2}$		$\langle z^2\rangle_A^{1/2}$		$\langle z^2\rangle_B^{1/2}$		$(c_{AB}/c_B)_{\rm est}$	
α_A	Numer.	TFA	Numer.	TFA	Numer.	TFA	Numer.	TFA	Value	Error (%)
10^1	1.1053	0.9013	1.0411	1.0061	0.9695	0.3662	1.6973	1.7100	0.7827	−26.163
10^2	1.5755	1.4284	1.6021	1.5946	1.0151	0.5804	2.7023	2.7102	0.9624	−9.203
10^3	2.3155	2.2639	2.5292	2.5272	1.1663	0.9199	4.2918	4.2954	1.0276	−3.053
10^4	3.5987	3.5880	4.0062	4.0054	1.5629	1.4579	6.8064	6.8078	1.0516	−0.789
10^5	5.6867	5.6867	6.3485	6.3481	2.3478	2.3107	10.7891	10.7896	1.0581	−0.178
10^6	9.0117	9.0128	10.0611	10.0610	3.6742	3.6622	17.1002	17.1004	1.0596	−0.037
10^7	14.2838	14.2843	15.9456	15.9456	5.8078	5.8041	27.1022	27.1022	1.0599	−0.007

density ϕ_A^2 shown in Fig. 3(c) is observed to have a highly oblate profile due to its coupling to species B; this suggests that the shape of the cloud carries a strong signal of the interspecies interaction, and consequently we may expect $(c_{AB}/c_B)_{\rm est}$ to be particularly accurate in this configuration. Indeed, its relative error $(c_{AB}/c_B)_{\rm est}\, c_B/c_{AB} - 1$ is only -1.13% already at $\alpha_A = 10^4$ and becomes $< 10^{-4}$ at $\alpha_A = 10^7$.

VII. DISCUSSION

In summary, we have presented an analytical TF solution for a miscible two-species BEC confined in a three-dimensional harmonic trap; we derived a formula, given by Eq. (17), that enables one to determine the relative interspecies interaction strength c_{AB}/c_B from the knowledge of the RMS values of two coordinates in the density distribution of species-A atoms. The error in the value of c_{AB}/c_B obtained in this manner has two origins. One is the imperfectness of the TFA itself, while the other is the uncertainty in the experimental measurements.

We addressed the first origin by means of a numerical comparison between the estimate $(c_{AB}/c_B)_{\rm est}$ obtained by applying Eq. (17) to the GP solution and the exact value c_{AB}/c_B. Although $(c_{AB}/c_B)_{\rm est}$ was found to be highly inaccurate for small numbers of condensed atoms, its relative error became smaller than or comparable to typical experimental uncertainties at atom numbers achievable at state-of-the-art experiments.

With regard to the second origin of error, we note that the masses and trap frequencies are typically known to a high accuracy (for example, by measuring the dipole oscillations of the center of mass of the atomic cloud, the relative uncertainty in determining the trap frequency can be as small as 10^{-3} [58, 61]). Consequently, the experimental uncertainty in evaluating the right-hand side of Eq. (17) arises mainly from the uncertainty in the measurement of $\delta_{ll'}^A \equiv \langle l^2\rangle_A/\langle l'^2\rangle_A$. Let its measurement be repeated N_δ times with the same accuracy (the same set of instruments). The result from the jth measurement is denoted by $\left(\delta_{ll'}^A\right)_j$. From the N_δ measurements we

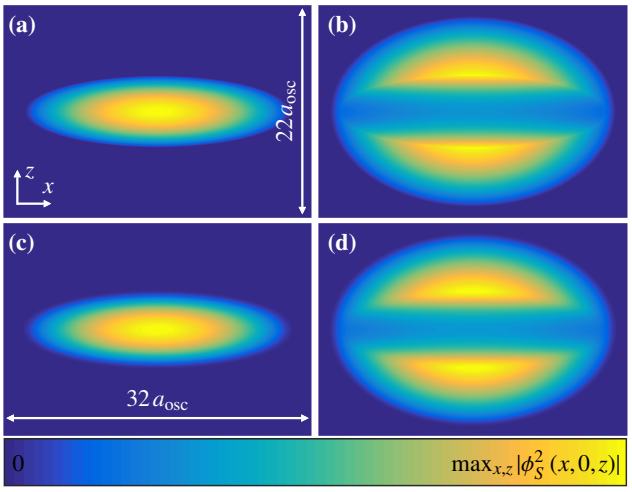

Figure 2. (a)–(b) Analytical TF and (c)–(d) numerical GP solutions for the cylindrically symmetric two-species BEC corresponding to the sixth entry in Table I, with $\alpha_A = 10^5$, and to the dotted curves in Fig. 1. Panels (a) and (c) show $|\phi_A^2|$, while panels (b) and (d) are for $|\phi_B^2|$. Here $a_{\rm osc} = \sqrt{\hbar/(m_A\omega_{Ax})}$. Each atomic density is rotationally symmetric about the z axis and is presented here in the plane $y = 0$. Evaluating the right-hand side of Eq. (17) for the GP solution shown in panels (c) and (d) yields the estimate $(c_{AB}/c_B)_{\rm est} = 0.7907$, which is 1.13% smaller than the true value 0.8.

obtain the mean value $\overline{\delta^A_{ll'}} = N_\delta^{-1}\sum_{j=1}^{N_\delta}\left(\delta^A_{ll'}\right)_j$. Following the standard procedure, we then quantify the uncertainty of $\delta^A_{ll'}$ in terms of the corrected sample standard deviation

$$\Delta\left[\delta^A_{ll'}\right] = \frac{1}{\sqrt{N_\delta - 1}}\left\{\sum_{j=1}^{N_\delta}\left[\left(\delta^A_{ll'}\right)_j - \overline{\delta^A_{ll'}}\right]^2\right\}^{1/2}. \qquad (19)$$

Furthermore, let the uncertainty in c_{AB}/c_B be denoted as $\Delta_{\{\omega_{Sl}\}}[c_{AB}/c_B]$, where the subscript $\{\omega_{Sl}\}$ specifies a fixed set of trap frequencies used in the measurements. As long as $\Delta\left[\delta^A_{ll'}\right]$ is small enough, from Eq. (17) we have

$$\Delta_{\{\omega_{Sl}\}}[c_{AB}/c_B] = \frac{m_A}{m_B}\frac{|\omega_{Bl}^2\omega_{Al'}^2 - \omega_{Al}^2\omega_{Bl'}^2|}{\left(\omega_{Bl'}^2 - \omega_{Bl}^2\overline{\delta^A_{ll'}}\right)^2}\Delta\left[\delta^A_{ll'}\right]. \qquad (20)$$

If we use the TF value Y_{Az}/Y_{Ax} in place of $\overline{\delta^A_{xz}}$ [see Eq. (16)], the coefficient on the right-hand side of Eq. (20) becomes 1.25×10^{-2} for the parameter set of Table I and 9.62×10^{-3} for that of Table II.

It follows from Eqs. (19) and (20) that the uncertainty in c_{AB}/c_B could be reduced by increasing the number N_δ of $\delta^A_{ll'}$ measurements or by choosing the set $\{\omega_{Sl}\}$ so as to make the numerator in Eq. (20) small [while ensuring that the conditions for the validity of Eq. (17) are not violated]. We could also adopt a number, say N_ω, of different sets of trap frequencies $\{\omega_{Sl}^{(j)}\}_{j=1}^{N_\omega}$ for the experiment. If the relative interaction strength was then determined as the average $\overline{c_{AB}/c_B} = N_\omega{}^{-1}\sum_j^{N_\omega}(c_{AB}/c_B)_j$, where $(c_{AB}/c_B)_j$ is the value obtained with the jth set, then the uncertainty in c_{AB}/c_B could be further reduced by increasing N_ω.

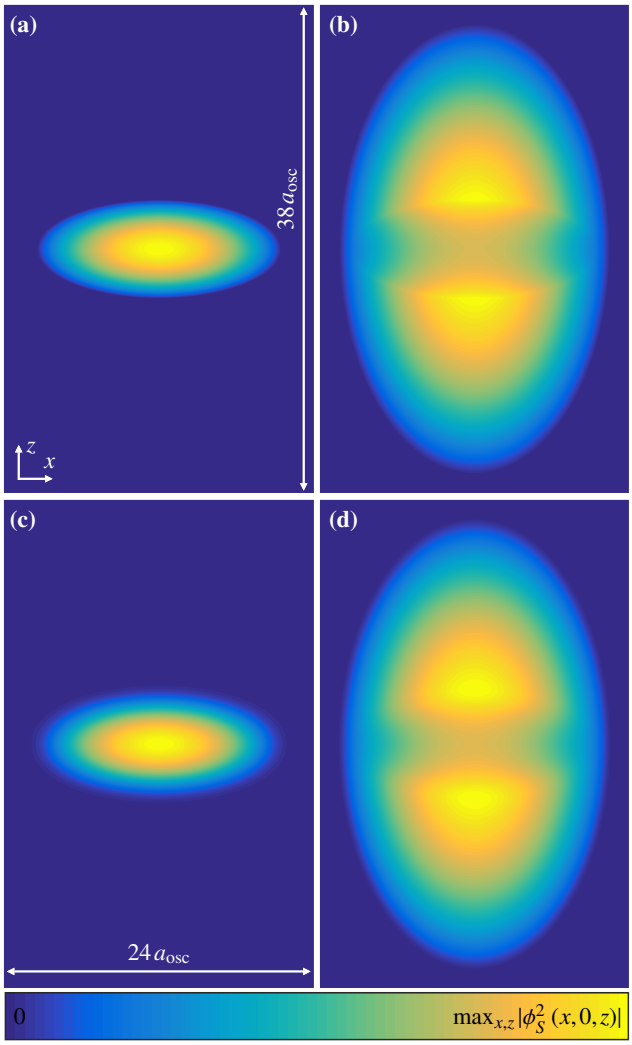

Figure 3. As Fig. 2, but for the fourth entry in Table II, with $\alpha_A = 10^4$. Applying Eq. (17) to the numerically obtained GP solution in panels (c) and (d) yields the estimate $(c_{AB}/c_B)_{\rm est} = 1.0516$, which is 0.79% smaller than the exact value 1.06.

To date, the most precise experimental determination of c_{AB}/c_B has been achieved through the measurement of collective oscillation frequencies in a two-species BEC of ^{87}Rb [58]. Various other condensate-based experiments [61–63], as well as ones involving collisional measurements on thermal samples [1, 59], have been performed to determine the interspecies scattering lengths. Nevertheless, Eq. (17) could still provide an additional way of determining the interspecies interaction strength, complementary to the existing methods. On the other hand, Eq. (17), or other analogous relations derivable from our TF solution, could also be used to cross-check the consistency of the observed density profiles against the assumed interaction strengths or other parameters of the solution, without the need to carry out time-consuming three-dimensional GP simulations.

The basic approach of forming piecewise-defined TF solutions of multispecies BECs is quite general [45] and can be applied to many more situations besides the one considered here.

In future work, it would be beneficial to derive the detailed TF solutions for the entire parameter space and investigate whether similar convenient relations could be found outside the validity range of the present solution. Such a general solution would also facilitate a detailed study of the ground-state phase diagram of the system. Another possible future extension could also be to apply the present approach to mixtures of two *spinor* condensates [64–67] instead of scalar ones.

Finally, it should be noted that besides inherently limiting the study to dilute zero-temperature gases, the underlying GP equations (1) have neglected effects that may be important in some situations. These could include, e.g., the axial misalignment or gravity-induced center offset of the two harmonic traps, the presence of finite-range interactions, or distortion of the density profiles due to losses from two- and three-body inelastic collisions.

ACKNOWLEDGMENTS

Useful comments from Dr. Zheng Wei are highly appreciated. This work is supported by the Technology Industries of Finland Centennial Foundation; the Academy of Finland under Grant No. 308632; the National Natural Science Foundation of China under Grants No. 11372122, 11274393, 11574404, and 11275279; the Open Project Program of State Key Laboratory of Theoretical Physics, Institute of Theoretical Physics, Chinese Academy of Sciences, China; and the National Basic Research Program of China (2013CB933601).

[1] G. Ferrari, M. Inguscio, W. Jastrzebski, G. Modugno, G. Roati, and A. Simoni, Phys. Rev. Lett. **89**, 053202 (2002).
[2] G. Modugno, M. Modugno, F. Riboli, G. Roati, and M. Inguscio, Phys. Rev. Lett. **89**, 190404 (2002).
[3] G. Thalhammer, G. Barontini, L. De Sarlo, J. Catani, F. Minardi, and M. Inguscio, Phys. Rev. Lett. **100**, 210402 (2008).
[4] K. Aikawa, D. Akamatsu, J. Kobayashi, M. Ueda, T. Kishimoto, and S. Inouye, New J. Phys. **11**, 055035 (2009).
[5] J. Catani, G. Barontini, G. Lamporesi, F. Rabatti, G. Thalhammer, F. Minardi, S. Stringari, and M. Inguscio, Phys. Rev. Lett. **103**, 140401 (2009).
[6] D. J. McCarron, H. W. Cho, D. L. Jenkin, M. P. Köppinger, and S. L. Cornish, Phys. Rev. A **84**, 011603 (2011).
[7] A. Lercher, T. Takekoshi, M. Debatin, B. Schuster, R. Rameshan, F. Ferlaino, R. Grimm, and H.-C. Nägerl, Eur. Phys. J. D **65**, 3 (2011).
[8] B. Pasquiou, A. Bayerle, S. M. Tzanova, S. Stellmer, J. Szczepkowski, M. Parigger, R. Grimm, and F. Schreck, Phys. Rev. A **88**, 023601 (2013).
[9] L. Wacker, N. B. Jørgensen, D. Birkmose, R. Horchani, W. Ertmer, C. Klempt, N. Winter, J. Sherson, and J. J. Arlt, Phys. Rev. A **92**, 053602 (2015).
[10] F. Wang, X. Li, D. Xiong, and D. Wang, J. Phys. B: At. Mol. Opt. Phys. **49**, 015302 (2015).
[11] S. B. Papp, J. M. Pino, and C. E. Wieman, Phys. Rev. Lett. **101**, 040402 (2008).
[12] S. Sugawa, R. Yamazaki, S. Taie, and Y. Takahashi, Phys. Rev. A **84**, 011610 (2011).
[13] S. Stellmer, R. Grimm, and F. Schreck, Phys. Rev. A **87**, 013611 (2013).
[14] C. J. Myatt, E. A. Burt, R. W. Ghrist, E. A. Cornell, and C. E. Wieman, Phys. Rev. Lett. **78**, 586 (1997).
[15] D. S. Hall, M. R. Matthews, J. R. Ensher, C. E. Wieman, and E. A. Cornell, Phys. Rev. Lett. **81**, 1539 (1998).
[16] M. R. Matthews, B. P. Anderson, P. C. Haljan, D. S. Hall, C. E. Wieman, and E. A. Cornell, Phys. Rev. Lett. **83**, 2498 (1999).
[17] G. Delannoy, S. G. Murdoch, V. Boyer, V. Josse, P. Bouyer, and A. Aspect, Phys. Rev. A **63**, 051602 (2001).
[18] V. Schweikhard, I. Coddington, P. Engels, S. Tung, and E. A. Cornell, Phys. Rev. Lett. **93**, 210403 (2004).
[19] R. P. Anderson, C. Ticknor, A. I. Sidorov, and B. V. Hall, Phys. Rev. A **80**, 023603 (2009).
[20] E. Timmermans, Phys. Rev. Lett. **81**, 5718 (1998).
[21] P. Ao and S. T. Chui, Phys. Rev. A **58**, 4836 (1998).
[22] J. O. Indekeu, C.-Y. Lin, N. Van Thu, B. Van Schaeybroeck, and T. H. Phat, Phys. Rev. A **91**, 033615 (2015).
[23] A. Roy and D. Angom, Phys. Rev. A **92**, 011601 (2015).
[24] J. Polo, V. Ahufinger, P. Mason, S. Sridhar, T. P. Billam, and S. A. Gardiner, Phys. Rev. A **91**, 053626 (2015).
[25] S. T. Chui and P. Ao, Phys. Rev. A **59**, 1473 (1999).
[26] M. Trippenbach, K. Góral, K. Rzazewski, B. Malomed, and Y. Band, J. Phys. B: At. Mol. Opt. Phys. **33**, 4017 (2000).
[27] F. Riboli and M. Modugno, Phys. Rev. A **65**, 063614 (2002).
[28] A. A. Svidzinsky and S. T. Chui, Phys. Rev. A **67**, 053608 (2003).
[29] S. Gautam and D. Angom, J. Phys. B: At. Mol. Opt. Phys. **43**, 095302 (2010).
[30] B. Van Schaeybroeck and J. O. Indekeu, Phys. Rev. A **91**, 013626 (2015).
[31] E. J. Mueller and T.-L. Ho, Phys. Rev. Lett. **88**, 180403 (2002).
[32] K. Kasamatsu, M. Tsubota, and M. Ueda, Phys. Rev. Lett. **93**, 250406 (2004).
[33] K. Kasamatsu, M. Tsubota, and M. Ueda, Phys. Rev. A **71**, 043611 (2005).
[34] K. Kasamatsu, M. Tsubota, and M. Ueda, Int. J. Mod. Phys. B **19**, 1835 (2005).
[35] S.-J. Yang, Q.-S. Wu, S.-N. Zhang, and S. Feng, Phys. Rev. A **77**, 033621 (2008).
[36] K. Kasamatsu and M. Tsubota, Phys. Rev. A **79**, 023606 (2009).
[37] P. Mason and A. Aftalion, Phys. Rev. A **84**, 033611 (2011).
[38] P. Kuopanportti, J. A. M. Huhtamäki, and M. Möttönen, Phys. Rev. A **85**, 043613 (2012).
[39] P. Kuopanportti, N. V. Orlova, and M. V. Milošević, Phys. Rev. A **91**, 043605 (2015).
[40] P. N. Galteland, E. Babaev, and A. Sudbø, New J. Phys. **17**, 103040 (2015).
[41] If the finite size and inhomogeneity of the system are neglected, the miscible regime corresponds to $|c_{AB}| < \sqrt{c_A c_B}$.
[42] As per standard nomenclature, a trap with $\omega_{Sx} \neq \omega_{Sy} \neq \omega_{Sz} \neq \omega_{Sx}$ will be referred to as *triaxial*.
[43] B. D. Esry, C. H. Greene, J. P. Burke, Jr., and J. L. Bohn, Phys. Rev. Lett. **78**, 3594 (1997).
[44] H. Pu and N. P. Bigelow, Phys. Rev. Lett. **80**, 1130 (1998).
[45] T.-L. Ho and V. B. Shenoy, Phys. Rev. Lett. **77**, 3276 (1996).
[46] M. Edwards and K. Burnett, Phys. Rev. A **51**, 1382 (1995).
[47] G. Baym and C. J. Pethick, Phys. Rev. Lett. **76**, 6 (1996).

[48] Roughly speaking, if we define the healing length $\xi_S = \hbar\{2m_S \max_{\mathbf{r}}[c_S n_S(\mathbf{r}) + c_{AB} n_{\$}(\mathbf{r})]\}^{-1/2}$, the geometric mean harmonic oscillator length $a_{S0} = \hbar^{1/2} m_S^{-1/2} \omega_{Sx}^{-1/6} \omega_{Sy}^{-1/6} \omega_{Sz}^{-1/6}$, and the geometric mean TF radius $R_{S0} = R_{Sx}^{1/3} R_{Sy}^{1/3} R_{Sz}^{1/3}$, where $R_{Sx} = \sup\{|x| \mid \exists (y,z) \text{ s.t. } \phi_S^2(x,y,z) > 0 \text{ for the TF solution}\}$ (with R_{Sy} and R_{Sz} defined analogously), then the TFA should be accurate as long as the separation of the length scales $\xi_S \ll a_{S0} \ll R_{S0}$ holds for both species $S \in \{A, B\}$.

[49] C. J. Pethick and H. Smith, *Bose-Einstein Condensation in Dilute Gases* (Cambridge University Press, Cambridge, 2008).

[50] Z. B. Li, Y. M. Liu, D. X. Yao, and C. G. Bao, J. Phys. B: At. Mol. Opt. Phys. **50**, 135301 (2017).

[51] Y.-Z. He, Y.-M. Liu, and C.-G. Bao, Comm. Theor. Phys. **68**, 220 (2017).

[52] C. Chin, R. Grimm, P. Julienne, and E. Tiesinga, Rev. Mod. Phys. **82**, 1225 (2010).

[53] A. Marte, T. Volz, J. Schuster, S. Dürr, G. Rempe, E. G. M. van Kempen, and B. J. Verhaar, Phys. Rev. Lett. **89**, 283202 (2002).

[54] M. Erhard, H. Schmaljohann, J. Kronjäger, K. Bongs, and K. Sengstock, Phys. Rev. A **69**, 032705 (2004).

[55] A. Widera, O. Mandel, M. Greiner, S. Kreim, T. W. Hänsch, and I. Bloch, Phys. Rev. Lett. **92**, 160406 (2004).

[56] C. D'Errico, M. Zaccanti, M. Fattori, G. Roati, M. Inguscio, G. Modugno, and A. Simoni, New J. Phys. **9**, 223 (2007).

[57] T. Kishimoto, J. Kobayashi, K. Noda, K. Aikawa, M. Ueda, and S. Inouye, Phys. Rev. A **79**, 031602 (2009).

[58] M. Egorov, B. Opanchuk, P. Drummond, B. V. Hall, P. Hannaford, and A. I. Sidorov, Phys. Rev. A **87**, 053614 (2013).

[59] M. Anderlini, E. Courtade, M. Cristiani, D. Cossart, D. Ciampini, C. Sias, O. Morsch, and E. Arimondo, Phys. Rev. A **71**, 061401 (2005).

[60] Note that the system satisfies $c_{AB}^2 < c_A c_B$ and is in the miscible regime.

[61] K. M. Mertes, J. W. Merrill, R. Carretero-González, D. J. Frantzeskakis, P. G. Kevrekidis, and D. S. Hall, Phys. Rev. Lett. **99**, 190402 (2007).

[62] M. R. Matthews, D. S. Hall, D. S. Jin, J. R. Ensher, C. E. Wieman, E. A. Cornell, F. Dalfovo, C. Minniti, and S. Stringari, Phys. Rev. Lett. **81**, 243 (1998).

[63] A. Widera, F. Gerbier, S. Fölling, T. Gericke, O. Mandel, and I. Bloch, New J. Phys. **8**, 152 (2006).

[64] M. Luo, Z. Li, and C. Bao, Phys. Rev. A **75**, 043609 (2007).

[65] M. Luo, C. Bao, and Z. Li, J. Phys. B: At. Mol. Opt. Phys. **41**, 245301 (2008).

[66] Z. F. Xu, Y. Zhang, and L. You, Phys. Rev. A **79**, 023613 (2009).

[67] Y. Shi and L. Ge, Phys. Rev. A **83**, 013616 (2011).